Research article

The Gd_2O_3 – $GdSrFeO_4$ pseudo -binary phase diagram

K.M. Kenges [a],[**],[1], A.A. Krasilin [b], E.A. Tugova [b],[*],[1]

[a] Center of Physical-Chemical Methods of Research and Analysis, Al-Farabi Kazakh National University, Almaty, Kazakhstan
[b] Ioffe Institute, 26 Politekhnicheskaya, St. Petersburg 194021, Russian Federation

A B S T R A C T

The Gd_2O_3 – $GdSrFeO_4$ pseudo-binary phase diagram is presented for the first time. The liquidus and eutectic temperatures, metatectic points of the Gd_2O_3 transformations in the Gd_2O_3 – $GdSrFeO_4$ section were defined using the Schröder–Le Chatelier equation, neglecting the effect of the isobaric heat capacity. The calculations were based on experimental data on the melting points of the end-members and the eutectic composition. From the results of phase relationships studies (subsolidus and high temperature region including literature data as well) and the above approach the Gd2O3–GdSrFeO4 pseudo-binary phase diagram in the temperature range 1400–2410 °C in air was constructed.

It was shown that $GdSrFeO_4$ of the K_2NiF_4- type is stable from 1100°C to a congruent melting temperature of 1560°C in air. The Gd_2O_3 – $GdSrFeO_4$ system is eutectic with no intermediate compounds.

1. Introduction

Ferrites based on perovskite and Ruddlesden–Popper (RP) structure are attracting increasing attention as oxygen permeable membranes [1,2], high-T_c oxides [3], high temperature fuel cells [4–13], coal-fire magnetohydrodynamic generators [14,15], etc. The ceramic materials being considered are generally well studied, but for new systems the phase relations are usually unknown; therefore, the phase equilibria study should be a major part of the materials development. The thermal stability of the perovskite-like $GdSr_2FeO_5$ and RP compounds $GdSrFeO_4$, $Gd_2SrFe_2O_7$ in the $GdO_{1.5}$ – SrO – $FeO_{1.5}$ ternary system has so far not been explored as well. The behavior and interaction of the components of the $GdO_{1.5}$ – SrO – $FeO_{1.5}$ system in a wide temperature range can be of practical interest, since they are included, among other things, in the composition of sacrificial materials [16,17].

The formation of three complex oxides with the perovskite-like structure: $Gd_2SrFe_2O_7$ ($GdFeO_3$: SrO = 2:1), $GdSrFeO_4$ ($GdFeO_3$: SrO = 1:1), $GdSr_2FeO_5$ ($GdFeO_3$: SrO = 1:2) located in $GdFeO_3$ – SrO section, as well as limited solid solutions of $Gd_{1-x}Sr_xFeO_{3-\alpha}$, $Gd_{1-x}Sr_{1+x}FeO_4$, $Gd_{2-x}Sr_{1+x}Fe_2O_7$ was established in the subsolidus region of the $GdO_{1.5}$ – SrO – $FeO_{1.5}$ system (Fig. 1) [18–26]. No previous works have been done on the $GdO_{1.5}$ – SrO – $FeO_{1.5}$ system at high temperature. The literature survey on thermal stability, heat fusion or melting temperatures of the studied compounds ($GdSr_2FeO_5$, $GdSrFeO_4$, $Gd_2SrFe_2O_7$) showed the absence of data also.

In the present work we focused on thermal stability of $GdSrFeO_4$. $GdSrFeO_4$ belongs to the Ruddlesden-Popper phases with the general chemical formula $AA'BO_4$ (where A^{+3} = Rare-earth metal cation, A'^{+2} = alkaline-earth metal cation; B is Al or 3d metal).
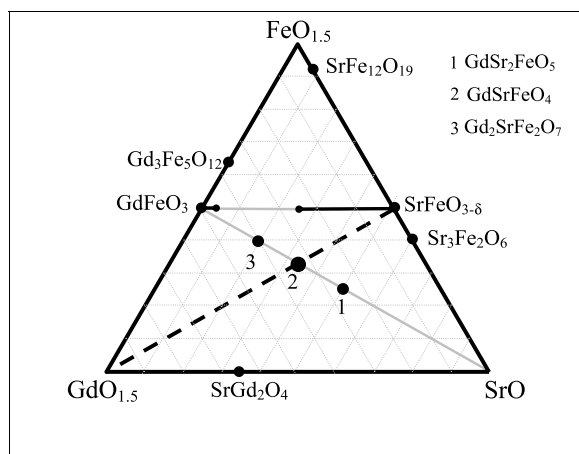
Fig. 1. Scheme illustrating the subsolidus phase relations in the $GdO_{1.5}$ – SrO – $FeO_{1.5}$ system in air at 1400 °C [16]. The section considered in the work is shown as dot line.

Table 1
Chemicals used for sample preparation.

Chemical Name	Formulae	Structural type	Source	Purity according to Supplier, %
Gadolinium (III) oxide	Gd_2O_3	cubic modification	Chemcraft, Russia	99.99 %
Strontium carbonate	$SrCO_3$	aragonite type		99.99 %
Iron (III) oxide	Fe_2O_3	a-Al_2O_3		>99 %

$GdSrFeO_4$ crystallizes in the K_2NiF_4-type crystal structure (space group *I4/mmm*) and consists of perovskite-like $GdFeO_3$ sheets interleaved by rock-salt like SrO layers [27–29]. The subsolidus relations study in the $GdO_{1.5}$ – $SrFeO_{3-\delta}$ pseudobinary section (Fig. 1) showed the presence of only one compound formed: $GdSrFeO_4$. $GdSrFeO_4$ was observed to form at 1100 °C through the interaction of Gd_2O_3 and $SrFeO_{3-\delta}$ [20,21]. No previous works have been done on phase equilibrium in the Gd_2O_3 – $SrFeO_{3-\delta}$ system research in the high temperature region as such, but Gd_2O_3 thermal behavior has been studied [30–33]. Gd_2O_3 crystallizes in five polymorphic forms: low-temperature cubic (C), monoclinic (B), hexagonal (A), high-temperature hexagonal (H) and cubic phases (X) [30–33].

We have therefore conducted a systematic study of phase equilibria in the $GdO_{1.5}$ – $SrFeO_{3-\delta}$ system, which is relevant for the applications described above. Here the Gd_2O_3 – $GdSrFeO_4$ pseudo-binary phase diagram is presented.

2. Experimental

$GdSrFeO_4$ was prepared by a conventional solid phase ceramic synthesis from Gd_2O_3, Fe_2O_3 and $SrCO_3$ powders (Table 1).

On the initial stage of the synthesis, the reagents were calcined at 1000°C for 2 h (Gd_2O_3), and at 300°C for 2 h ($SrCO_3$ and Fe_2O_3) prior to use. A correction for $SrCO_3$ decarbonization was calculated using thermogravimetric data [18,19]. To synthesize single-phase $GdSrFeO_4$, an excess of 5 mol. % $SrCO_3$ was added over the stoichiometry of $GdSrFeO_4$. The choice is due to a number of experiments based on literature data [13,34,35] on synthetic complexities of $LnMBO_4$ (Ln = rare earth element; M = Mg, Ca, Sr, Ba; B=Al, Fe, Co) series. The main goal was to change the synthesis scheme of $GdSrFeO_4$ to avoid the by-product $Gd_2SrFe_2O_7$ formation [20]. Mixtures of reagents were weighed, then homogenized with a small amount of water and dried. The resulting powder was micromilled in an agate mortar and pressed into pellets at a pressure of 500 MPa. The pellets were sintered in air at 1100–1400 °C varying exposure times from 5 to 35 h to study the formation mechanism and achieve a single-phase target product. The pellets were rapidly cooled to room temperature in air at the end of each heat treatment.

Room temperature powder X-ray diffraction (XRD) patterns of samples were recorded using powder X-ray diffractometer Shimadzu XRD-7000 with the CoK_α radiation.

The microstructure and elemental composition of $GdSrFeO_4$ after synthesis and melting were analyzed by scanning electron microscopy (SEM) and energy dispersive X-ray spectroscopy (EDS) using a Quanta 200 scanning electron microscope equipped with an X-ray microanalyzer. The content of elements normalized to 100% was calculated using the ZAF correction procedure.

The Mössbauer spectrum of $GdSrFeO_4$ was acquired at room temperature; the ^{57}Co isotope in the Rh matrix was used as a source (WissEl Mössbauer spectrometer, Wissenschaftliche Elektronik GmbH, Germany). The isomer shift value was determined relative to α-Fe.

The thermal stability of $GdSrFeO_4$ was investigated by visual thermal analysis on original design setup – a high-temperature microscope. A powder sample was placed in the middle of a U-shaped heater-holder composed of iridium wire. The experiments were carried out in air $P_{O_2} = 0.21 \cdot 10^5 Pa$. Visible changes in the sample were captured using a high-speed camera. The melting temperature
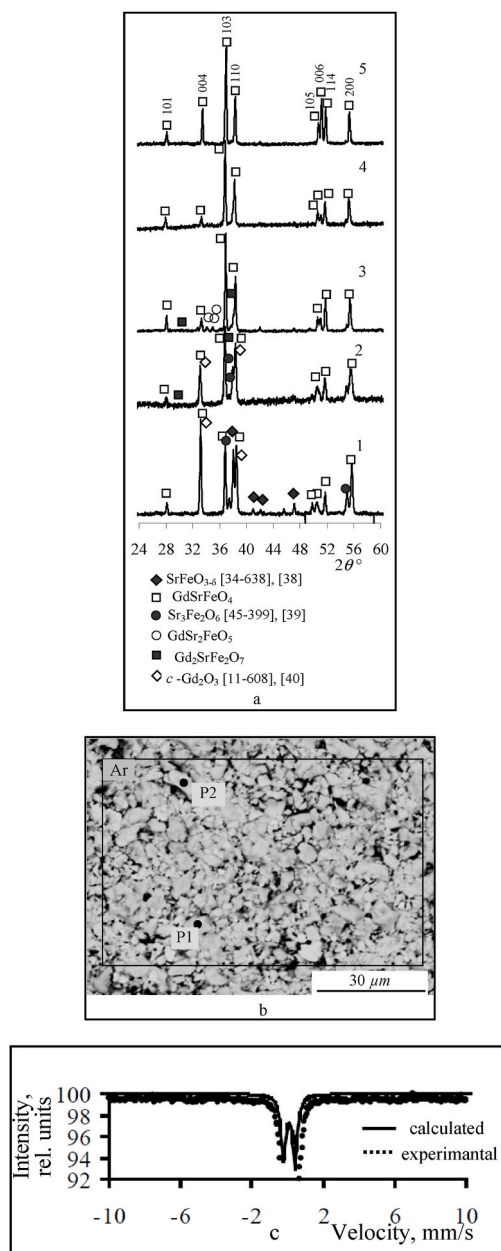
Fig. 2. a) XRD patterns of samples heat treated in air at 1) 1100 °C, 2) 1200 °C, 3) 1300 °C, 4) 1400 °C for 5 h, and 5) 1400 °C for 35 h; b) scanning electron microscopy images and c) room Mössbauer spectrum of $GdSrFeO_4$ synthesized at 1400 °C for 35 h [**-***] means ICDD database.

was determined as the temperature at which the melt was spread over the looped holder. The errors in determining the melting temperature did not exceed 20 °C. More detailed construction of the high-temperature microscope and the measurement techniques have been described in Refs. [36,37].

3. Results and discussion

The X-Ray results of samples (Fig. 2 a) heat treated at 1100–1300 °C for 5 h indicated the formation of target product $GdSrFeO_4$ along with $SrFeO_{3-\delta}$ [38], $Sr_3Fe_2O_6$ [39], $GdSr_2FeO_5$, $Gd_2SrFe_2O_7$ in small amounts, and the residual quantity of unreacted Gd_2O_3 [40]. According to XRD data (Fig. 2 a), the further increase of sintering temperature up to 1400°C, as well as exposure time for 5 h and 35 h led to the single-phase $GdSrFeO_4$ preparation. The applied approach showed the change of $GdSrFeO_4$ synthesis scheme with the $GdSr_2FeO_5$ formation at the beginning and its subsequent interaction with $Gd_2SrFe_2O_7$. The second possible formation mechanism of $GdSrFeO_4$ was proposed: 1/3 $GdSr_2FeO_5$ + 1/3 $Gd_2SrFe_2O_7$═$GdSrFeO_4$.

Table 2
Phases found by EDS in synthesized and cooled down from melt GdSrFeO$_4$ samples.

Sample (Fig.)[a]	Analyzed area	Sample composition (mol%)			Phases observed
		FeO$_{1.5}$	SrO	GdO$_{1.5}$	
Fig. 2 *b*	Ar	32.66	35.00	32.34	GdSrFeO$_4$
	P1	32.13	34.85	33.02	
	P2	33.65	34.40	31.95	
Fig. 3	Ar	32.68	35.19	32.12	GdSrFeO$_4$
	Ar1	28.93	29.95	41.12	Eutectics,
	Ar2	28.75	30.85	40.40	GdSrFeO$_4$ + Gd$_2$O$_3$
	Ar3	29.18	28.38	42.44	
	Ar4	27.77	29.19	43.04	
	Ar5	28.90	30.10	41.00	
	Ar6	30.77	30.77	38.46	
	P1	14.48	18.67	66.31	Gd$_2$O$_3$
	P2	14.05	20.39	65.56	
	P3	30.05	38.51	31.43	GdSrFeO$_4$
	P4	34.87	37.25	27.88	
	P5	33.38	36.20	30.42	
	P6	33.30	34.85	31.86	
	P7	31.43	37.14	31.43	
	P8	32.32	35.57	32.11	
	P9	32.35	35.18	32.46	
	P10	30.68	37.09	32.27	

[a] Sample designation correlates with the micrographs presented in Figs. 2b and 3.

Table 3
Mössbauer spectrum parameters of GdSrFeO$_4$.

Oxide	Fe ion	Isomer shift, mm/s	Quadrupole splitting, mm/s	Content, %
GdSrFeO$_4$	Fe^{+3}	0.33 ± 0.01	1.02 ± 0.01	100

Data used.

The X-ray data of GdSrFeO$_4$ synthesized at 1400 °C for 35 h showed only the tetragonal GdSrFeO$_4$ (Fig. 2 a, b, Tabl. 2) [20,22]. The GdSrFeO$_4$ formation of the stoichiometric composition along with the X-Ray data and spectral microanalysis was confirmed by the Mössbauer spectroscopy (Fig. 2 c, Tabl. 3). Single-phase GdSrFeO$_4$ Mössbauer spectrum (Fig. 2 *c*) showed the presence of one doublet. Mössbauer spectrum parameters of GdSrFeO$_4$ are given in Table 3. Iron atoms were in a high-spin paramagnetic state, Fe^{+3}, as evidenced by the given values of the isomer shift (Table 3).

Fig. 3 shows micrographs reflecting the GdSrFeO$_4$ crystallization under melting produced by high-temperature microscope. According to the SEM/EDS data, small eutectic areas of (GdSrFeO$_4$+Gd$_2$O$_3$) (Ar 1-Ar 6, Table 2) in the matrix of GdSrFeO$_4$ (P3–P10, Table 2) as well as particles of the Gd$_2$O$_3$-based phase (P1, P2 Table 2) were determined. These Gd$_2$O$_3$-bases particles are mostly located close to the eutectic areas. The eutectic microstructure is closed to dendrite-like. The composition of eutectic was measured to be FeO$_{1.5}$, SrO ~30 mol. % and GdO$_{1.5}$–40 mol.% (Table 2), or when converted to complex oxides: 57 mol.% GdO$_{1.5}$–43 mol.% SrFeO$_{3-\delta}$ or 15 mol.% Gd$_2$O$_3$ – 85 mol.% GdSrFeO$_4$. The chemical composition of these regions, determined by the EDS method (Table 2), had similar values, which also confirmed their macrohomogeneous character. GdSrFeO$_4$ melted congruently based on the invariance of the composition before and after fusion. The melting temperature of the considered compound was determined to be 1560 ± 20 °C. The result obtained was consistent with the decreasing melting temperatures trend for known ferrites LnSrFeO$_4$ from 1900 °C (for Ln = La) [41], 1740 °C (Ln = Nd) [36] to 1535 °C (Ln = Eu) [42].

As mentioned above, no previous works have been done on the Gd$_2$O$_3$ – SrFeO$_{3-\delta}$ system or its Gd$_2$O$_3$ – GdSrFeO$_4$ section in the high temperature region. It is of interest to calculate the phase diagram for this system on the assumption that it is eutectic. If the ideal solution laws are assumed, it is possible to calculate the phase diagram for such pseudo-binary system.

3.1. Methodologies for determining liquidus and eutectic temperatures

The liquidus and eutectic temperatures, the metatectic points composition were estimated using the empirical Schröder–Le Chatelier equation, neglecting the influence of the isobaric heat capacity.

For an ideal solution (and assuming that no solid solubility occurs) it can be written:

$$\ln x_{l_i} = \frac{\Delta H_{m_i}^*}{R}\left(\frac{1}{T_{m_i}^*} - \frac{1}{T_{l_i}}\right),$$

where R = 8.31 J K^{-1} mol^{-1}; T_{l_i} stands for the liquidus temperature when the GdSrFeO$_4$ component is added to the Gd$_2$O$_3$ component,
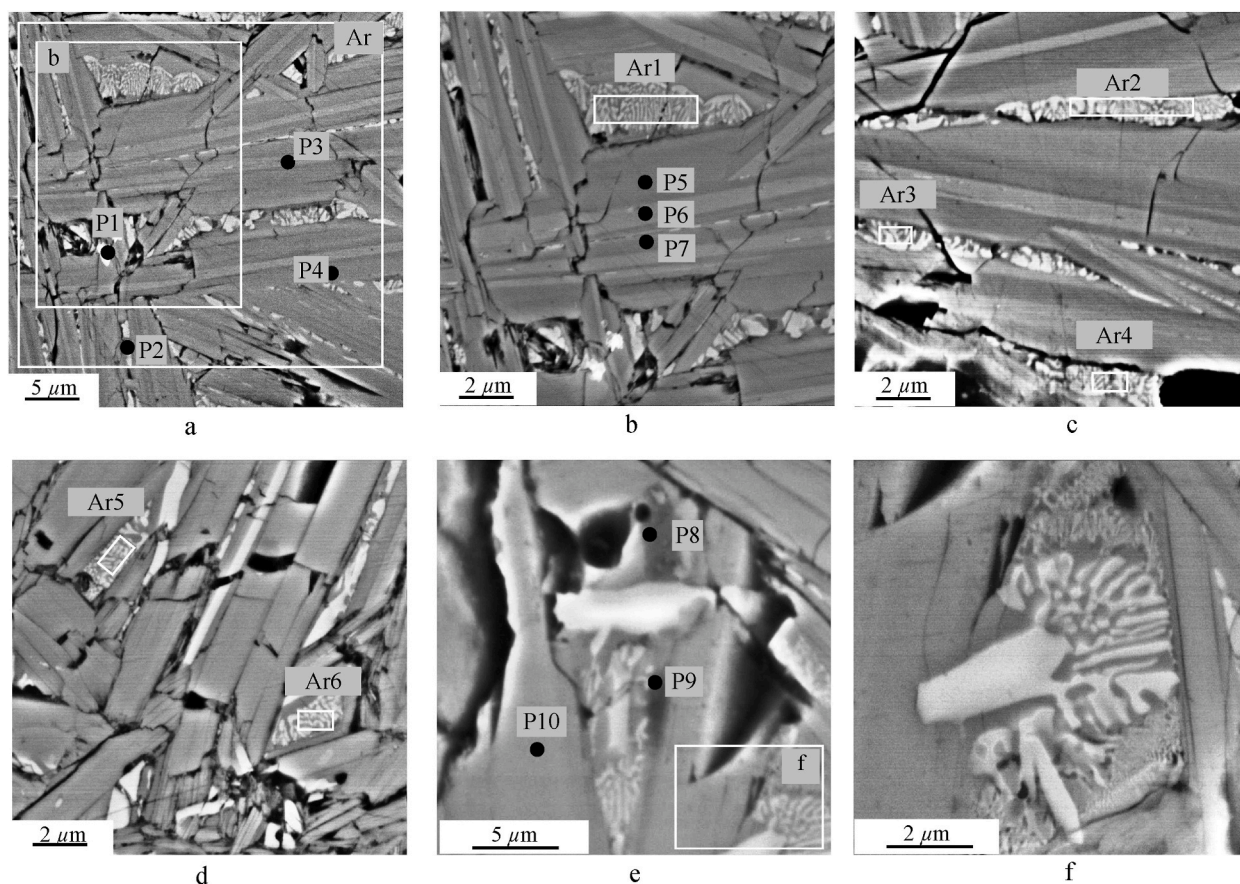
Fig. 3. Microstructure image of GdSrFeO$_4$ crystallization after fusion.

Table 4
Summary of the temperature and enthalpies of discrete transitions: C→B, B→A, A→H, H→X and X→L for Gd$_2$O$_3$. ASS: assessment; EST: estimation.

Gd$_2$O$_3$ Phase transitions	Source [31–33]/Techniques						
	[31]/EST		[32]/EST		[33]/ASS		
	T$_{tr}$ (°C)	ΔH$_{tr}$. KJ/mol	T$_{tr}$ (°C)	ΔH$_{tr}$. KJ/mol	T$_{tr}$ (°C)	ΔH$_{tr}$. KJ/mol	[a]x_{l_i}
C↔B	1152	5.325	–	9.0	1288	6.68	–
B↔A	2170	6.300	2157	6.3	2110	3.40	0.66
A↔H	2208	34.7	2197	34.7	2174	6.12	0.73
H↔X	2360	12.03	2265	20.5	2369	6.61	0.95
X↔L	2420	71.702	2420	92.0	2410	67.21	–

Note.

C – low-temperature cubic.

B –monoclinic.

A –hexagonal.

H – high-temperature hexagonal.

X – high-temperature cubic phase.

[a] This work estimation done using the Schroder–Le Chatelier equation.

K; x_{l_i} is mole fraction of the ith component, $\Delta H_{m_i}^*$ is the heat of fusion of the Gd$_2$O$_3$ component (J/(mol); $T_{m_i^*}$ is the new calculated "imaginary" melting temperature required to determine the cusp of the liquidus curve when phase transitions of gadolinium oxide are taken into account.

The initial data used for calculation were the melting temperatures of the end-members Gd$_2$O$_3$ and GdSrFeO$_4$ of the Gd$_2$O$_3$ – GdSrFeO$_4$ system, as well as data on the Gd$_2$O$_3$ phase transitions temperatures and heats [31–33,43], summarized in Table 4. The Gd$_2$O$_3$ heats of fusion are not known with any degree of reliability, so we proceeded from the assumption that the article from Ref. [33]
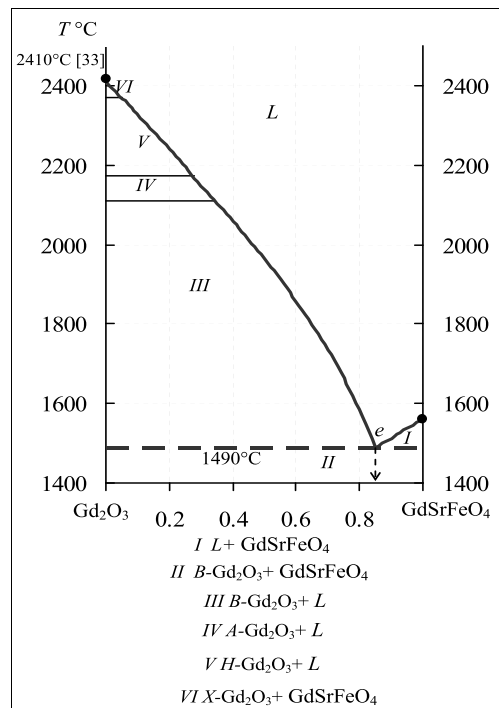
Fig. 4. Isobaric Gd$_2$O$_3$ – GdSrFeO$_4$ pseudo-binary phase diagram.

contained full analysis of previous works [31,32]. Besides the performed T_e calculations with data on transition and fusion heats taken from Refs. [31,32] led to false results: to the elevated eutectic temperatures: 1690 °C and 1780 °C, respectively.

Procedure for the step-by-step calculation of metatectic points composition and liquidus temperature was following: to calculate the composition of metatectic points at the phase transition at 2369 °C, the data of Table 4 were used: $\ln x_{l_1} = \frac{67210}{8.314}\left(\frac{1}{2683} - \frac{1}{2642}\right)$.

Further, the sum of the melting and phase transition heats at 2369 °C and the composition defined in the previous step were taken to determine $T^*_{m_1}$: $\ln 0.95 = \frac{67210+6610}{8.314}\left(\frac{1}{T^*_{m_1}} - \frac{1}{2642}\right)$. For mentioned calculations took $T_{l_i} = T_{tr_i}$ - phase transition temperature. According to this example x_{l_2}, $T^*_{m_2}$, x_{l_3}, $T^*_{m_3}$ were successively determined, and then, on the basis of the last values, taking into account the composition of the eutectic determined from the experiment, T_e was defined. Thus the course of the liquidus curve was received.

The eutectic point is located at 1490 °C and 85 mol.% GdSrFeO$_4$ in the Gd$_2$O$_3$ – GdSrFeO$_4$ system, based on Schröder-Le Chatelier equation calculation. The former requires confirmation. The phase transformations of Gd$_2$O$_3$ X↔H ↔ A ↔ B display on the liquidus curve as metatectic points at 2369 °C and 95 mol% Gd$_2$O$_3$, 2174 °C and 73 mol% Gd$_2$O$_3$, and 2110 °C and 66 mol% Gd$_2$O$_3$, respectively (Table 4). The phase transformation of Gd$_2$O$_3$ B ↔ C takes place at 1288 °C and does not display on the liquidus of the Gd$_2$O$_3$ – GdSrFeO$_4$ system. Using these data and the equations above, the phase diagram can be computed. This has been done and the results have been plotted in Fig. 4. The eutectic line was drawn by a dotted line. The predicted GdSrFeO$_4$ heat of fusion was determined to be 62524.64 J/mol based on Schröder–Le Chatelier equation.

4. Conclusion

As the study result, the two GdSrFeO$_4$ formation mechanisms were proposed: ½ Gd$_2$O$_3$ + SrFeO$_{3-\delta}$ as well as 1/3 Gd$_2$SrFe$_2$O$_7$ + 1/3GdSr$_2$Fe$_2$O$_5$. The formation of GdSrFeO$_4$ through the interaction of Gd$_2$O$_3$ and SrFeO$_{3-\delta}$ is considered to be more appropriate.

For the first time the melting temperature and character of GdSrFeO$_4$ were determined. GdSrFeO$_4$ melts congruently at 1833 K (1560 °C). Assuming that thermal effects do not depend on temperature the liquidus lines of the Gd$_2$O$_3$–GdSrFeO$_4$ pseudo-binary were calculated using the Schroeder–Le Chatelier method. From the results of phase relationships studies (subsolidus and high temperature regions) and the above approach the Gd$_2$O$_3$–GdSrFeO$_4$ pseudo-binary phase diagram in the temperature range 1400–2410 °C in air was constructed. The eutectic point is at 1490 °C and 85 mol.% GdSrFeO$_4$ in the Gd$_2$O$_3$ – GdSrFeO$_4$ system, based on the Schröder-Le Chatelier equation calculation. The limitations of this calculation should not exceed 6 mol. % and 50 °C, taking into account the errors of each method. The eutectic microstructure was closed to the dendrite-like. The predicted GdSrFeO$_4$ heat of fusion was estimated to be ~62.5 kJ/mol. The obtained data can be used to enlarge the thermodynamic database for oxide systems as well.

Funding

Data availability statement

All the data analysis results obtained during this study are included in the manuscript. Any additional information required to reanalyze the data reported in this work is available from the lead contact upon request.

CRediT authorship contribution statement

K.M. Kenges: Writing – review & editing, Software, Funding acquisition. **A.A. Krasilin:** Writing – review & editing, Methodology. **E.A. Tugova:** Writing – original draft, Supervision, Investigation, Conceptualization.

Declaration of competing interest

The authors declare that they have no known competing financial interests or personal relationships that could have appeared to influence the work reported in this paper.

Acknowledgements

References

[1] Z. Liu, K. Li, H. Zhao, K. Świerczek, High-performance oxygen permeation membranes: cobalt-free $Ba_{0.975}La_{0.025}Fe_{1-x}Cu_xO_{3-\delta}$ ceramics, J. Materiomics. 5 (2019) 264–272, https://doi.org/10.1016/j.jmat.2019.01.013.

[2] X. Zhu, W. Yang, Chapter 12 - Critical factors affecting oxygen permeation through dual-phase membranes, in: S.T. Oyama, S.M. Stagg-Williams (Eds.), Membr. Sci. Technol., Elsevier, 2011, pp. 275–293, https://doi.org/10.1016/B978-0-444-53728-7.00012-4.

[3] A.N. Kovalenko, High-temperature superconductivity: from macro to nanoscale structures, Nanosystems, Phys. Chem. Math 7 (6) (2016) 941–970, https://doi.org/10.17586/2220-8054-2016-7-6-941-970.

[4] A.V. Nikonov, K.A. Kuterbekov, K.Z. Bekmyrza, N.B. Pavzderin, A brief review of conductivity and thermal expansion of perovskite-related oxides for SOFC cathode, Eurasian J. Phys. Funct. Mater. 2 (2018) 274–292, https://doi.org/10.29317/ejpfm.2018020309.

[5] P. Ding, W. Li, H. Zhao, C. Wu, L. Zhao, B. Dong, S. Wang, Review on Ruddlesden–Popper perovskites as cathode for solid oxide fuel cells, J. Phys. Mater. 4 (2021) 022002, https://doi.org/10.1088/2515-7639/abe392.

[6] M.A. Yatoo, S.J. Skinner, Ruddlesden-Popper phase materials for solid oxide fuel cell cathodes: a short review, Mater. Today Proc. 56 (2022) 3747–3754, https://doi.org/10.1016/j.matpr.2021.12.537.

[7] ShI. Elkalashy, A.R. Gilev, T.V. Aksenova, A.S. Urusova, V.A. Cherepanov, Phase equilibria, structure and properties of complex oxides in the $NdFeO_{3-\delta}$ – $SrFeO_{3-\delta}$ – $SrCoO_{3-\delta}$ – $NdCoO_{3-\delta}$ system as potential cathodes for SOFCs, Solid State Ionics 316 (2018) 85–92, https://doi.org/10.1016/j.ssi.2017.12.028.

[8] G. Nirala, D. Yadav, S. Upadhyay, Ruddlesden-Popper phase A_2BO_4 oxides: recent studies on structure, electrical, dielectric, and optical properties, J. Adv. Ceram. 9 (2020) 129–148, https://doi.org/10.1007/s40145-020-0365-x.

[9] D. Muñoz Gil, K. Boulahya, M. Santamaria Santoyo, M.T. Azcondo, U. Amador, Superior performance as cathode material for intermediate-temperature solid oxide fuel cells of the ruddlesden–popper n = 2 member $Eu_2SrCo_{0.50}Fe_{1.50}O_{7-\delta}$ with low cobalt content, Inorg. Chem. 60 (2021) 3094–3105, https://doi.org/10.1021/acs.inorgchem.0c03391.

[10] J. Oliva, C.R. Garcia, E. Verduzco, A.I. Martinez, A. Manthiram, K.P. Padmasree, Enhancing the photocatalytic activity of the perovskite-based intergrowth oxide $Sr_{3.2}La_{0.8}Fe_{1.5}Co_{1.5}O_{10-\delta}$ with Ca substitution, Ceram. Int. 43 (2017) 14074–14081, https://doi.org/10.1016/j.ceramint.2017.07.143.

[11] T. Ghorbani-Moghadam, A. Kompany, M. Golmohammad, Study of structural, electrical and electrochemical properties of $La_{0.7}Sr_{1.3}Co_{1-x}Fe_xO_4$ (x = 0, 0.1, 0.3, 0.5) Ruddlesden-Popper oxides as promising cathode for intermediate solid oxide fuel cells, J. Alloys Compd. 900 (2022) 163382, https://doi.org/10.1016/j.jallcom.2021.163382.

[12] A.K. Baral, Y. Tsur, V. Thangadurai, Electrochemical studies of Ruddlesden-Popper layered perovskite-type $La_{0.6}Sr_{1.4}Co_{0.2}Fe_{0.8}O_{4+\delta}$ cathode for solid oxide fuel cells and associated electrical loss phenomena, Ceram. Int. 45 (2019) 1641–1650, https://doi.org/10.1016/j.ceramint.2018.10.041.

[13] K.M. Kenges, E.A. Tugova, Strategies for optimizing the single $GdSrFeO_4$ phase synthesis, Open Chem. 21 (1) (2023), https://doi.org/10.1515/chem-2023-0170. ArtNo: #20230170.

[14] T. Sasamoto, J. Mizusaki, M. Youshimura, W.R. Cannon, H.K. Bowen, Phase relationships and electrical conductivity of the perovskite-type solid solutions in the system $SrZrO_3$-$LaFeO_3$-$SrFeO_3$ in air, J. Ceram. Soc. Jpn. 90 (1) (1982) 24–30, https://doi.org/10.2109/jcersj1950.90.32.

[15] M.H. Sukkar, D.R. Sadoway, Electrical conductivity and thermal stability measurements of a mixed perovskite oxide system, J. Appl. Phys. 53 (1982) 3686–3689, https://doi.org/10.1063/1.331154.

[16] V.B. Khabensky, V.S. Granovsky, S.V. Bechta, V.V. Gusarov, Severe accident management concept of the VVER-1000 and the justification of corium retention in a crucible-type core catcher, Nucl. Eng. Technol. 41 (2009) 561–574, https://doi.org/10.5516/NET.2009.41.5.561.

[17] V.V. Gusarov, V.B. Khabensky, S.V. Bechta, V.S. Granovsky, V.I. Almjashev, E.V. Krushinov, S.A. Vitol, E.D. Sergeev, V.V. Petrov, V.A. Tikhomirov, V.V. Bezlepkin, I.V. Kukhtevich, YuN. Aniskevich, I.V. Sayenko, V.L. Stolyarova, V.P. Migal, V.A. Mozherin, V.Ya Sakulin, A.N. Novikov, G.N. Salagina, E.A. Shtern, V.G. Asmolov, S.S. Abalin, YuG. Degaltsev, V.N. Zagryazkin. CN1500274 Oxide material for molten-core catcher of nuclear reactor. https://patentscope.wipo.int/search/en/detail.jsf?docId=CN82691930&_cid=P20-LJ2R07-56367-1 (accessed June 19, 2023).

[18] E.A. Tugova, Phase Formation in the $GdFeO_3$–SrO system at 1200–1400°? Glass Phys. Chem. 48 (2022) 614–621, https://doi.org/10.1134/S1087659622600454.

[19] E.A. Tugova, A.A. Krasilin, V.V. Panchuk, V.G. Semenov, V.V. Gusarov, Subsolidus phase equilibria in the $GdFeO_3$-$SrFeO_{3-\delta}$ system in air, Ceram. Int. 46 (2020) 24526–24533, https://doi.org/10.1016/j.ceramint.2020.06.239.

[20] E.A. Tugova, V.V. Gusarov, Peculiarities of layered perovskite-related $GdSrFeO_4$ compound solid state synthesis, J. Alloys Compd. 509 (2011) 1523–1528, https://doi.org/10.1016/j.jallcom.2010.10.149.

[21] I.V. Otrepina, V.S. Volodin, I.A. Zvereva, J.-Sh Liu, Investigation of the formation of the GdSrFeO4 oxide, Glass Phys. Chem. 35 (2009) 423–430, https://doi.org/10.1134/S1087659609040129.

[22] S. Singh, D. Singh, Effect of increasing Sr content on structural and physical properties of K_2NiF_4-type phase GdSrFeO4, Ceram. Int. 43 (2017) 3369–3376, https://doi.org/10.1016/j.ceramint.2016.11.182.

[23] T.F. Sheshko, T.A. Kryuchkova, YuM. Serov, I.V. Chislova, I.A. Zvereva, New mixed perovskite-type $Gd_{2-x}Sr_{1+x}Fe_2O_7$ catalysts for dry reforming of methane, and production of light olefins, Catal. Ind. 9 (2017) 162–169, https://doi.org/10.1134/S207005041702009X.

[24] A.M. Sankovich, I.V. Chislova, A.V. Blokhin, M.D. Bal'makov, I.A. Zvereva, Low-temperature calorimetric study of layered perovskite-like ferrites GdSrFeO4 and $Gd_2SrFe_2O_7$, J. Therm. Anal. Calorim. 126 (2016) 601–608, https://doi.org/10.1007/s10973-016-5542-3.

[25] L.V. Khvostova, N.E. Volkova, L.Ya Gavrilova, A. Maignan, V.A. Cherepanov, Gd_2O_3–SrO–Fe_2O_3 system: the phase diagram and oxygen content in oxides, Mater. Today Commun. 29 (2021) 102885, https://doi.org/10.1016/j.mtcomm.2021.102885.

[26] J. Christopher, C.S. Swamy, Studies on the catalytic decomposition of N_2O on LnSrFeO4 (Ln=La, Pr, Nd, Sm and Gd), J. Mol. Catal. 68 (1991) 199–213, https://doi.org/10.1016/0304-5102(91)80075-E.

[27] B.V. Beznosikov, K.S. Aleksandrov, Perovskite-like crystals of the ruddlesden-popper series, crystallogr, Rep 45 (2000) 792–798, https://doi.org/10.1134/1.1312923.

[28] S.N. Ruddlesden, P. Popper, New compounds of the K_2NiF_4 type, Acta Crystallogr. 10 (1957) 538–539, https://doi.org/10.1107/S0365110X57001929.

[29] J.C. Joubert, A. Collomb, D. Elmaleh, G. Le Flem, A. Daoudi, G. Ollivier, Sur quelques nouveaux oxydes mixtes de strontium et d'éléments de transition du type K_2NiF_4, J. Solid State Chem. 2 (1970) 343–346, https://doi.org/10.1016/0022-4596(70)90092-7.

[30] P.P. Fedorov, M.V. Nazarkin, R.M. Zakalyukin, On polymorphism and morphotropism of rare earth sesquioxides, Crystallogr. Rep. 47 (2002) 281–286, https://doi.org/10.1134/1.1466504.

[31] M. Zinkevich, Thermodynamics of rare earth sesquioxides, Prog. Mater. Sci. 52 (2007) 597–647, https://doi.org/10.1016/j.pmatsci.2006.09.002.

[32] R.J.M. Konings, O. Beneš, A. Kovács, D. Manara, D. Sedmidubský, L. Gorokhov, V.S. Iorish, V. Yungman, E. Shenyavskaya, E. Osina, The thermodynamic properties of the f-elements and their compounds. Part 2. The lanthanide and actinide oxides, J. Phys. Chem. Ref. Data 43 (2014) 013101, https://doi.org/10.1063/1.4825256.

[33] Y. Zhang, I.-H. Jung, Critical evaluation of thermodynamic properties of rare earth sesquioxides (RE = La, Ce, Pr, Nd, Pm, Sm, Eu, Gd, Tb, Dy, Ho, Er, Tm, Yb, Lu, Sc and Y), Calphad 58 (2017) 169–203, https://doi.org/10.1016/j.calphad.2017.07.001.

[34] A.E. Becerra-Toledo, L.D. Marks, Strontium oxide segregation at SrLaAlO4 surfaces, Surf. Sci. 604 (17–18) (2010) 1476–1480, https://doi.org/10.1016/j.susc.2010.05.011.

[35] M. Sanchez-Andujar, M.A. Senaris-Rodriguez, Synthesis, structure and microstructure of the layered compounds $Ln_{1-x}Sr_{1+x}CoO_4$ (Ln: La, Nd and Gd), Solid State Sci. 6 (2004) 21–27, https://doi.org/10.1016/j.solidstatesciences.2003.11.005.

[36] E.A. Tugova, Phase transformations in the $Nd_2SrAl_2O_7$–$Nd_2SrFe_2O_7$ system, Russ. J. Inorg. Chem. 67 (2022) 874–880, https://doi.org/10.1134/S0036023622060237.

[37] A.A. Komlev, V.I. Almjashev, S.V. Bechta, V.B. Khabensky, V.S. Granovsky, V.V. Gusarov, New sacrificial material for ex-vessel core catcher, J. of Nuclear Materials. 467 (2015) 778–784, https://doi.org/10.1016/j.jnucmat.2015.10.035.

[38] F. Haberey, A. Kockel, The formation of strontium hexaferrite $SrFe_{12}O_{19}$ from pure iron oxide and strontium carbonate, IEEE Trans. Magn. 12 (1976) 983–985, https://doi.org/10.1109/TMAG.1976.1059205.

[39] E. Lucchini, D. Minichelli, G. Sloccari, The crystal structure of α-$Sr_3Fe_2O_{7-x}$, Acta Crystallogr. B 29 (1973) 2356–2357, https://doi.org/10.1107/S0567740873006692.

[40] C.E. Curtis, J.R. Johnson, Ceramic properties of samarium oxide and gadolinium oxide; X-ray studies of other rare-earth oxides and some compounds, J. Am. Ceram. Soc. 40 (1957) 15–19, https://doi.org/10.1111/j.1151-2916.1957.tb12541.x.

[41] E.A. Tugova, V.F. Popova, I.A. Zvereva, V.V. Gusarov, Phase diagram of the LaFeO3-LaSrFeO4 system, Glass Phys. Chem. 32 (6) (2006) 674–676, https://doi.org/10.1134/S1087659606060137.

[42] M. Drofenik, D. Kolar, L. Golič, Phase relations in the system SrO-Eu_2O_3-Fe_2O_3 and a new ternary phase Sr_2EuFeO_5, J. Less Common. Met. 37 (1974) 281–284, https://doi.org/10.1016/0022-5088(74)90043-5.

[43] S.V. Ushakov, P.S. Maram, D. Kapush, A.J. Pavlik, M. Fyhrie, L.C. Gallington, C.J. Benmore, R. Weber, J.C. Neuefeind, J.W. McMurray, A. Navrotsky, Phase transformations in oxides above 2000°C: experimental technique development, Adv. Appl. Ceram. 117 (2018) s82–s89, https://doi.org/10.1080/17436753.2018.1516267.